A Kapitza–Dirac–Talbot–Lau interferometer for highly polarizable molecules

STEFAN GERLICH[1], LUCIA HACKERMÜLLER[1]*, KLAUS HORNBERGER[2], ALEXANDER STIBOR[1†], HENDRIK ULBRICHT[1], MICHAEL GRING[1], FABIENNE GOLDFARB[1‡], TIM SAVAS[3], MARCEL MÜRI[4], MARCEL MAYOR[4,5] AND MARKUS ARNDT[1§]

[1]Faculty of Physics, University of Vienna, Boltzmanngasse 5, A-1090 Wien, Austria
[2]Arnold Sommerfeld Center for Theoretical Physics, Ludwig-Maximilians-Universität München, Theresienstrasse 37, 80333 München, Germany
[3]Nanostructures Laboratory, Massachusetts Institute of Technology, 77 Massachusetts Avenue, Cambridge, Massachusetts 02139-4307, USA
[4]University of Basel, Department of Chemistry, St Johannsring 19, CH-4056 Basel, Switzerland
[5]Forschungszentrum Karlsruhe GmbH, Institute for Nanotechnology, PO Box 3640, D-76021 Karlsruhe, Germany
*Present address: Johannes Gutenberg-Universität Mainz, Staudingerweg 7, 55099 Mainz, Germany
†Present address: Phys. Institut der Universität Tübingen, Auf der Morgenstelle 14, D-72076 Tübingen, Germany
‡Present address: Laboratoire Aimé Cotton, CNRS-UPR 3321, Bat. 505, Campus Univ., F-91405 Orsay, France
§e-mail: markus.arndt@univie.ac.at

Published online: 19 August 2007; doi:10.1038/nphys701

Research on matter waves is a thriving field of quantum physics and has recently stimulated many investigations with electrons[1], neutrons[2], atoms[3], Bose-condensed ensembles[4], cold clusters[5] and hot molecules[6]. Coherence experiments with complex objects are of interest for exploring the transition to classical physics[7–9], for measuring molecular properties[10], and they have even been proposed for testing new models of space-time[11]. For matter-wave experiments with complex molecules, the strongly dispersive effect of the interaction between the diffracted molecule and the grating wall is a major challenge because it imposes enormous constraints on the velocity selection of the molecular beam[12]. Here, we describe the first experimental realization of a new set-up that solves this problem by combining the advantages of a so-called Talbot–Lau interferometer[13] with the benefits of an optical phase grating.

Several methods have been developed in the past for the coherent manipulation of matter waves with de Broglie wavelengths in the nanometre and picometre range. For instance, free-standing material gratings were used in the diffraction of electrons[14], atoms[15,16] and molecules[5,6,17]. In addition, coherent beam splitting at non-resonant standing light waves, often designated the Kapitza–Dirac effect, has been observed for all of these species[18–20].

Recent implementations of near-field interferometry[13,21–23] underlined the particular advantages of the Talbot–Lau concept for experiments with massive objects: the required grating period scales only weakly ($d \sim \sqrt{\lambda}$) with the de Broglie wavelength, and the design accepts beams of low spatial coherence, which makes high signals possible even for weak sources.

A symmetric Talbot–Lau interferometer (TLI) consists of three identical gratings. The first one prepares the transverse coherence of the weakly collimated beam. Quantum near-field diffraction at the second nanostructure generates a periodic molecular density distribution at the position of the third mask, which represents a self-image of the second grating, if the grating separation equals a multiple of the Talbot length $L_T = d^2/\lambda$. The mask can be laterally shifted to transform the molecular interference pattern into a modulation of the molecular beam intensity that is recorded behind the interferometer.

In the established TLI design with three nanofabricated gratings[23], the molecule–wall interaction with the grating bars imprints a further phase shift φ on the matter wave, which depends on the molecular polarizability α, the velocity v_z and the distance r to the wall within the grating slit. Because of its strongly nonlinear r-dependence, this interaction restricts the interference contrast to very narrow bands of de Broglie wavelengths, as we show in Fig. 1a for the example of the fullerene C_{70}. In this simulation, we use the full Casimir–Polder potential[24], even though the long-distance (retarded) approximation, decaying as α/r^4, closely reproduces the results. The sharply peaked blue line shows the expected interference fringe visibility as a function of the de Broglie wavelength for a TLI composed of three silicon nitride gratings with a period of 266.38 nm. The periodic recurrence of the fringe visibility with multiples of $\lambda = d^2/L$ is a generic feature of any such three-grating set-up. The grating separation was fixed to $L = 105$ mm. The left peak in Fig. 1a therefore corresponds to the fourth Talbot order for C_{70} at 175 m s^{-1}. The presence of the walls modifies the transmission function[25] and leads to a dramatic narrowing of the accepted width of the wavelength distribution, here corresponding to a velocity spread of $\Delta v/v_z = 0.7\%$ (full-width at half-maximum). This requirement has to be compared with available molecular beam methods: currently available sources for very massive neutral molecules only allow preparation of beams that exhibit either a velocity or mass spread (or both) of often significantly more than 10%. A better post-selection is conceivable in principle, but the existing sources generally provide an insufficient flux to allow this.

For more complex particles with larger polarizabilities, lower velocity and higher velocity spread than C_{70}, the phase shift in the presence of material walls will be even more important. We demonstrate this in Fig. 1b, where we simulate the expected fringe visibility for large perfluorinated molecules[26] in a conventional TLI.

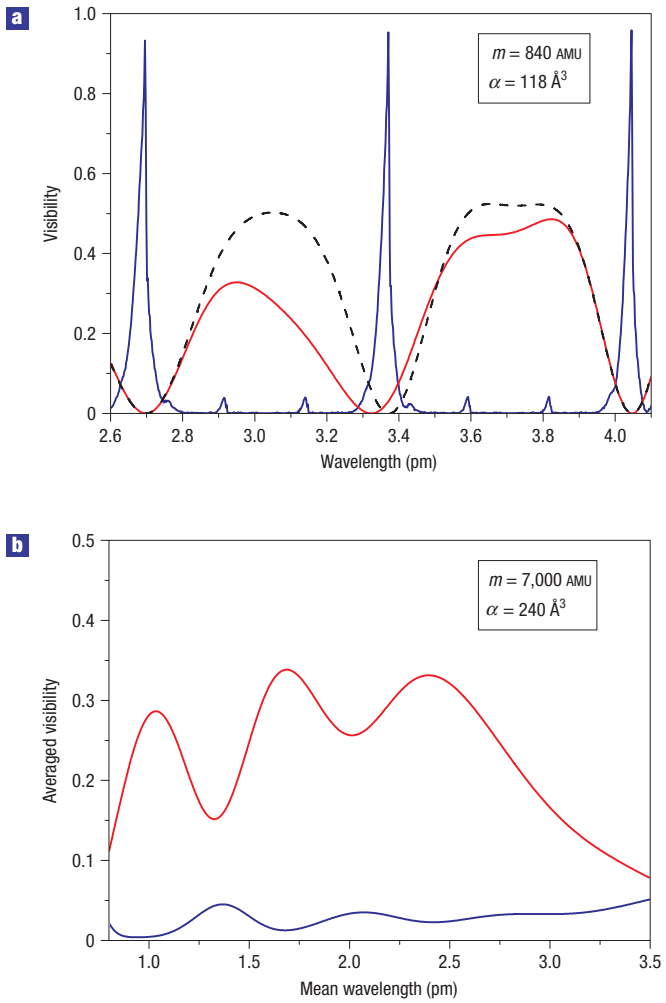

Figure 1 Numerical prediction of the interference fringe visibility as a function of the de Broglie wavelength: comparison of the TLI and the KDTLI for molecules of different complexity. a, Fullerene C_{70} contrast under the assumption of a monochromatic beam. The blue line shows the expected fringe visibility for a pure TLI set-up, that is, when only silicon nitride gratings are used in all three places. Only in a very narrow band of de Broglie wavelengths ($\Delta\lambda/\lambda < 0.7\%$ full-width at half-maximum) can the visibility reach significant values. In marked contrast to that, the $\Delta\lambda$ acceptance range of the KDTLI is more than ten times larger (dashed curve), even in the presence of a realistic photon absorption rate (red line). These curves are based on equation (1) with $P = 5$ W and $\sigma_{abs} = 2.1 \times 10^{-21}$ m^2. A wavelength average over a realistic velocity distribution of 10% (standard deviation) leads to a total fringe contrast of <5% for the TLI and up to 25% for the KDTLI set-up. **b**, Perfluorinated macromolecules. The interference visibility is wavelength averaged over an experimentally realistic distribution of mean velocities in the range of $v_z = 20$–70 m s^{-1} with $\Delta v/v_z = 10\%$. For such slow and polarizable particles, the fringe visibility of the KDTLI design (red line) at $P = 0.6$ W and $\sigma_{abs} = 1.34 \times 10^{-21}$ m^2 can clearly exceed that of the TLI design (blue line) by about a factor of ten.

The presence of dispersive interactions clearly reduces the expected fringe contrast to values of around 4% (blue line, Fig. 1b).

To circumvent the molecule–wall interaction, we now combine the Talbot–Lau concept with the idea of the Kapitza–Dirac effect, that is, with a standing light wave as the diffraction element.

Specifically, we replace the central grating by a standing laser light wave of period $d = \lambda_L/2$, which interacts with the molecules by the dipole force[20]. The spatially varying laser intensity thus induces an oscillating dipole moment shifting the phase of the matter wave in proportion to the local intensity and to α_L, the molecular polarizability at the laser wavelength λ_L. A phase grating constructed this way has several advantages: it is indestructible and it combines 100% transmission with a tunable phase shift. But most importantly, all parameters can be chosen to obtain a high interference contrast over a broad wavelength distribution as simulated in Fig. 1a (dashed line).

We note that the first and third gratings may remain as absorptive masks. The first grating selects a periodic set of slit sources from the molecular beam and thus prepares the required transverse coherence[23]. Similarly, the third mask provides the high spatial resolution in the detection of the periodic molecular interference pattern.

The molecule–wall interaction is also of minor relevance in both the entrance and the exit grating: the molecules enter the first grating without a well-defined phase and we observe only molecular flux, and not phase, behind the third nanostructure.

The molecule–laser interaction can be characterized by the phase Φ_{max} that is imprinted on the de Broglie wave at the position of the maxima of the standing light wave[20]

$$\Phi_{max} = \frac{8\sqrt{2\pi}\alpha_L}{\hbar c w_y v_z} P.$$

This amounts to $\Phi_{max} \sim \pi$ or C_{70} with a polarizability of $\alpha_L = 118$ Å^3 at $\lambda_L = 532$ nm, a molecular velocity of $v_z = 130$ m s^{-1}, a vertical laser beam waist of $w_y = 900$ μm and a laser power of $P = 5$ W.

In addition to this coherent effect of the laser potential, we also have to consider the possibility of photon absorption. Each absorbed photon adds a momentum kick of $\pm h/\lambda_L$ to the molecules and thus adds to the blur of the accumulated interference pattern. This incoherent interaction is characterized by the mean number of absorbed light quanta in the antinode

$$n_0 = \frac{8\sigma_{abs}\lambda_L}{\sqrt{2\pi}hcw_y v_z} P$$

and amounts in our example to $n_0 = 0.8$ photons per molecule, with the absorption cross-section $\sigma_{abs} = 2.1 \times 10^{-21}$ m^2 (ref. 27) and all other parameters as above.

A rigorous treatment within the framework of our previously established phase-space theory for the TLI[23,28] predicts that the interference pattern behind the Kapitza–Dirac–Talbot–Lau interferometer (KDTLI) will be described by a nearly sinusoidal curve of visibility

$$V = 2 \cdot \left(\frac{\sin(\pi f)}{\pi f}\right)^2 \cdot \exp(-\xi_{abs}) \cdot \frac{\xi_{coh} - \xi_{abs}}{\xi_{coh} + \xi_{abs}} \cdot J_2\left(-\mathrm{sgn}(\xi_{coh} + \xi_{abs})\sqrt{\xi_{coh}^2 - \xi_{abs}^2}\right). \quad (1)$$

Here the coherent diffraction parameter

$$\xi_{coh} = \Phi_{max} \sin\left(\pi \frac{L}{L_T}\right)$$

and the parameter of absorption

$$\xi_{abs} = n_0 \sin^2\left(\frac{\pi L}{2L_T}\right) \quad (2)$$

are determined by the grating separation L, the Talbot length L_T and the open fraction $f = 0.42$, that is, the ratio of slit size and

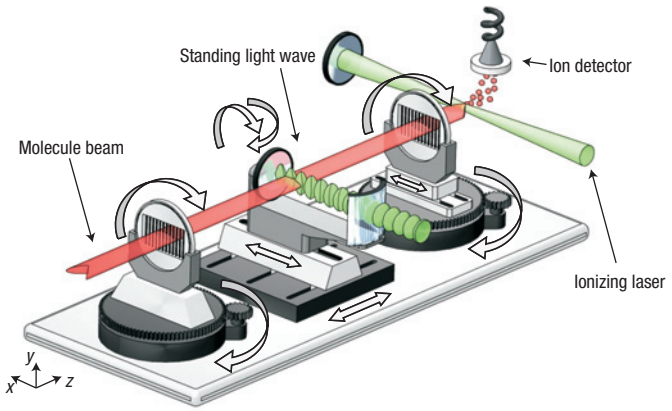

Figure 2 Schematic diagram of the KDTLI. The molecular beam, arriving from the left, passes the first nanograting which imposes a periodic spatial filtering and thus the required transverse coherence onto the molecular beam. The spatially varying potential of the standing light leads to a phase modulation of the matter wave, which results in a molecular density pattern at the position of the third grating. The latter is again a material mask of equal period and can be laterally shifted across the molecule beam to sample the interference pattern. High-vacuum motors are used to fine-adjust the roll angle of all gratings, their longitudinal separation, as well as the transverse shift of the third grating. C_{70} fullerenes are detected by laser ionization, as shown here. Perfluoroalkyl-functionalized azobenzenes are recorded using electron-impact ionization mass spectrometry.

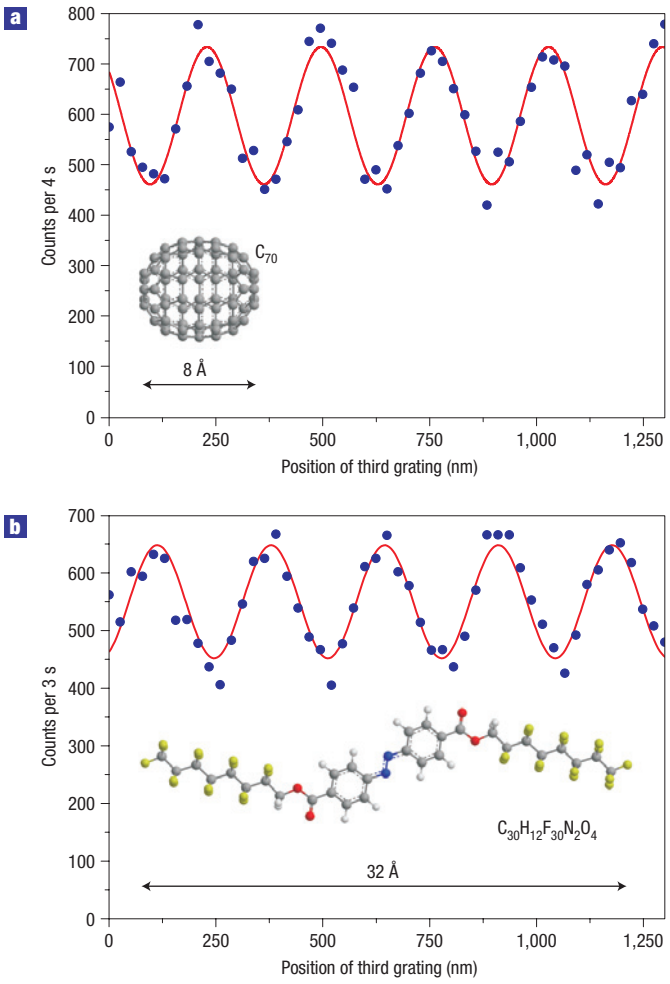

Figure 3 Typical interference patterns observed in KDTL interferometry. **a**, Interference fringes of C_{70}, recorded at a mean molecular velocity of 146 m s^{-1} ($\Delta v/v_z = 16\%$) and a diffraction laser power of 6 W. The red line is a sinusoidal fit. The observed fringe visibility of 23% is in good agreement with the expected values of Figs 1 and 4, when the appropriate velocity averaging is taken into account. **b**, Quantum interference with perfluoroalkyl-functionalized azobenzenes. The laser power was set to 7.3 W. The velocity distribution was centred at $v_z = 140$ m s^{-1} with a standard deviation of 25%. A dark count rate of 15 counts per second was subtracted. The experimental fringe visibility of 18.0% is in good agreement with the quantum theoretical expectation (18.5%) and three times higher than expected for a purely mechanical TLI. The fringe period is determined by the geometry of the set-up and is equal for the fullerenes and the azobenzenes. The insets in **a** and **b** show C_{70} and the stretched state of functionalized azobenzenes, respectively. A direct comparison reveals that the customized azobenzenes are up to four times more extended than the fullerenes. Their aspect ratio (length to diameter) can be about an order of magnitude larger than for C_{70}.

period in the nanofabricated gratings. J_2 designates the Bessel function of second order. In the limit of vanishing absorption ($\xi_{abs} \to 0$) it reduces to $J_2(\xi_{coh})$.

The red line in Fig. 1a shows the full effect of the laser interaction according to equation (1). We observe that the interference visibility is reduced, in particular for slow molecules which have more time to absorb a photon. Yet, the most important advantage of the KDTLI design, a significant interference contrast over a broad wavelength range, is clearly preserved.

We note that for many large molecules, from perfluorinated particles to large polypeptides, the absorption lines are blue-shifted with respect to those of fullerenes, and the ratio σ_{abs}/α_L at 532 nm can be more than ten times smaller than for C_{70} (ref. 27). For these objects the effect of absorption will be negligible and even higher fringe visibilities can be expected.

This is again demonstrated in Fig. 1b, where we simulate the interference contrast in our KDTLI set-up for perfluorinated molecules with $m = 7{,}000$ AMU. A comparison between this result (red line, Fig. 1b) and the prediction for purely matter gratings (blue line, Fig. 1b) reveals that our new set-up allows us to gain one order of magnitude in fringe visibility.

To validate the concept, we have implemented the interferometer for C_{70} as shown in the schematic diagram in Fig. 2. The molecular beam emerges from a thermal source. Its mean velocity can be selected using a previously established gravitational selection scheme[23] within the range of $v_z = 80$–200 m s^{-1} and with $\Delta v_z/v_z \sim 7$–20% (standard deviation). The molecules that pass the third grating are ionized by a green 18 W laser beam, which is focused to a waist of 15 μm in a double-pass arrangement. They are subsequently detected in an ion counter.

The free-standing gratings were photolithographically etched into a 190-nm-thick silicon nitride (SiN_x) membrane[29]. A crucial point in the preparation of the experiment is the precise matching of all three grating periods. Already an average deviation by as little as 0.05 nm, that is, by the radius of a single hydrogen atom, reduces the fringe visibility by one third.

In the experiment, we sample the interference curve by shifting the third grating laterally while counting the total number of transmitted molecules. Figure 3a shows exemplary interference fringes recorded with C_{70} in the KDTLI set-up.

From several such curves we then extract the fringe visibility of the interference signal as a function of the grating laser power. In Fig. 4, we compare the result with the predictions of equation (1), including the measured velocity spreads, for four different mean

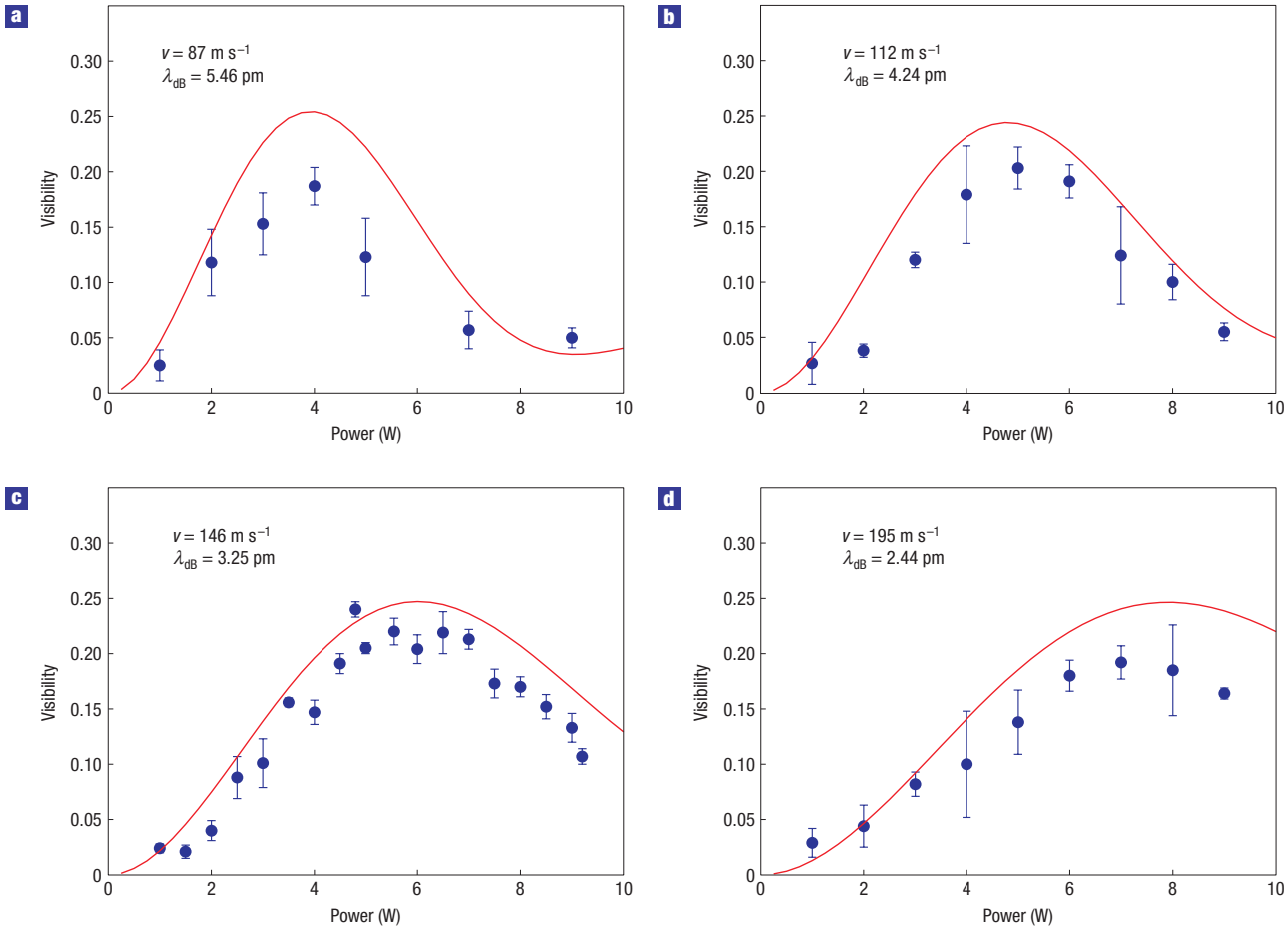

Figure 4 Dependence of the interference fringe contrast on the diffracting laser power. a–d, C_{70} interference visibility as a function of the diffraction laser power at four different molecule velocity distributions, with the following mean velocities v_z and velocity spreads Δv (standard deviation): $v_z = 87\,\mathrm{m\,s^{-1}}$, $\Delta v/v_z = 0.09$ (**a**), $v_z = 112\,\mathrm{m\,s^{-1}}$, $\Delta v/v_z = 0.13$ (**b**), $v_z = 146\,\mathrm{m\,s^{-1}}$, $\Delta v/v_z = 0.16$ (**c**) and $v_z = 195\,\mathrm{m\,s^{-1}}$, $\Delta v/v_z = 0.21$ (**d**). The circles mark the experimental results. The error bars correspond to the standard deviation of three consecutive measurements. The red lines represent the theoretical expectation of equation (1), including both the dispersive and the absorptive effects on the molecule–light interaction without any free parameters. We attribute the small remaining deviations between experiment and theory mainly to day-to-day variations of the vibrational noise in the laboratory. The centre of the peak shifts towards higher laser power for increasing velocities. This is related to the decreasing interaction time with the laser field.

molecular velocities. The experimental data validate our theoretical model to a very high degree and thereby also confirm the enormous precision in the manufacturing of the diffraction elements. Depending on the laser power we reach an interference contrast of up to 24%. This represents a significant improvement over a TLI with three material gratings, for which the visibility would remain below 6% at these broad velocity distributions.

The new instrument now allows us to demonstrate quantum interference with a new class of molecules, here with perfluoroalkyl-functionalized azobenzenes, which were synthesized for this specific purpose (see the Methods section and Supplementary Information). In their thermally preferred *trans*-conformation[30] (inset of Fig. 3b) they are about four times longer and also a bit more massive (∼1,030 AMU) than the fullerene C_{70}. Although the limited count rate forced us to work with a broad, nearly thermal velocity distribution ($\Delta v/v_z \approx 0.25$), we still see a good interference contrast that is very compatible with our quantum interference model (Fig. 3b).

All parameters of our present experimental set-up are still compatible with molecular beams in a mass range up to 11,000 AMU and velocities of $50\,\mathrm{m\,s^{-1}}$. Such experiments should become accessible in the near future by combining modern chemical synthesis with improved beam sources.

When we extrapolate the simulations for our set-up even to $Au_{5,000}$ clusters at cryogenic temperatures (∼10 K), we still predict a fringe visibility of 40% for a mass of $m \sim 1{,}000{,}000$ AMU, a polarizability of $\alpha \sim 25{,}000\,\text{Å}^3$, velocities in the range of $v_z \sim 1\,\mathrm{m\,s^{-1}}$ and a mass or velocity spread of up to 10%. Such an experiment represents a very worthy goal for future research, with interesting challenges related to the enormous sensitivity of such an interferometer to alignment, inertial forces and dephasing effects.

The Kapitza–Dirac–Talbot–Lau concept thus opens de Broglie interferometry to a very wide class of clusters and molecules in an unprecedented mass and complexity region.

Our demonstration with perfluoroalkyl-functionalized azobenzenes underlines in particular that such experiments can be carried out with realistic molecular beams, that is, also with a rather broad velocity distribution.

The new interferometer also leads to a number of applications, including tests of recent proposals on gravitational decoherence[11] or molecule metrology[10]. It is particularly interesting to note that azobenzenes and their derivatives are often used as molecular

switches, which change their conformation on absorption of a single photon[30]. It will therefore be intriguing to study the possibility of optically controlled conformational state changes on quantum interferometry and decoherence in the future.

METHODS

EXPERIMENTAL LAYOUT AND ALIGNMENT OF THE INTERFEROMETER

The KDTLI is composed of three gratings: two absorptive silicon nitride gratings and one optical phase grating. The optical grating was created by focusing a green single-mode laser beam (Coherent Verdi 10 W) with a cylindrical lens to a horizontal waist of $w_z = 20\,\mu$m onto a plane mirror, to create a standing light wave.

The Rayleigh length of the gaussian laser beam amounts to 2.4 mm, which is sufficiently long to keep the laser wavefront curvature small over the intersection region with the molecular beam. The vertical waist was set to $w_y = 900\,\mu$m to maximize the field homogeneity over the interaction region.

The laser has a fixed wavelength of 532.28 ± 0.01 nm, and the material gratings had to be tailored to half this value. They were manufactured to $d = 266.38 \pm 0.05$ nm and the effective grating period was tuned *in situ* by rotating the gratings around their vertical axes (see Fig. 2).

The molecular beam divergence and the beam alignment with respect to the mirror plane are restricted to about 1 mrad to avoid phase averaging over different nodal planes of the light wave.

All gratings were optically aligned to be parallel to each other to better than 300 μrad. The separations between two neighbouring gratings differ by less than 50 μm. Their distance was set to $L = 105$ mm. This corresponds to the first Talbot length for molecules with $m = 11{,}000$ AMU and $v_z = 50\,\mathrm{m\,s^{-1}}$ ($\lambda_{\mathrm{dB}} = 700$ fm). For C_{70}, it amounts to the fourth up to the eighth Talbot order, depending on the selected velocity.

To correctly include the average over a finite velocity distribution, the signal average is computed before we extract the corresponding visibility.

AZOBENZENE DERIVATIVE FUNCTIONALIZED WITH FLUORINATED ALKYL CHAINS

To minimize intermolecular attraction and hence to increase the compound's vapour pressure, an azobenzene derivative with fluorinated alkyl chains was synthesized by esterification of azobenzene 4,4′-dicarboxylic acid with a highly fluorinated alkyl alcohol (see the Supplementary Information). Azobenzene 4,4′-dicarboxylic acid was obtained at a yield of 83% by treating 4-nitrobenzoic acid with sodium hydroxide, D-glucose and air in water. The corresponding acid chloride derivative was obtained by treatment with thionyl chloride. Subsequent reaction with 1H-1H-perfluoro-1-octanol in dry tetrahydrofuran and triethylamine as a base afforded the desired azobenzene 4,4′-di(carboxylic acid 1″H-1″H-perfluoro-1″-octanolate) as an orange crystalline solid. The purification of the target structure by sublimation at 200 °C and a pressure of 2.7×10^{-2} mbar points to its considerably increased vapour pressure in spite of the mass of 1,034 AMU, a crucial physical property of the compound to obtain sufficient molecular beam intensities for matter-wave experiments. However, recrystallization from hot chloroform turned out to be the more efficient purification procedure with an isolated yield of 72%. The new compounds were characterized by NMR spectroscopy and mass spectrometry. Even though the fluorinated azobenzene is a new compound that has been designed and synthesized for this experiment, analogy with comparable derivatives allows us to predict particular structural features. Using 'Gaussian 03W V6.0 (Gaussian, 2003)', we determine the low-temperature scalar molecular polarizability of the stretched conformation to be 49 Å^3. On the basis of earlier comparisons between this program and our own molecule metrology experiments[10], we estimate the error to be smaller than 20%. In addition to their high vapour pressure due to the fluorinated alkyl chains, azobenzene derivatives are known for their reversible photoisomerization[30] between the thermodynamically favourable *trans* form (Fig. 3b) and the folded *cis* form. An understanding of the high-temperature dynamics of these conformations will require further computational modelling.

We used electron-impact ionization and quadrupole mass spectrometry (CMS Extrel Merlin 1…4000 u) to detect these molecules after their passage through the interferometer. This allowed us to select molecules with a mass resolution of $\Delta m/m < 1\%$ and we still get a sufficient signal for interferometry, under the condition that we open the beam to a vertical height of 400 μm and broaden the velocity spread to $\Delta v/v_z = 0.25$ (standard deviation $\mathrm{m\,s^{-1}}$).

Received 26 February 2007; accepted 25 July 2007; published 19 August 2007.

References

1. Ji, Y. *et al.* An electronic Mach–Zehnder interferometer. *Nature* **422**, 415–418 (2003).
2. Hasegawa, Y., Loidl, R., Badurek, G., Baron, M. & Rauch, H. Violation of a Bell-like inequality in single neutron interferometry. *Nature* **425**, 45–48 (2003).
3. Schumm, T. *et al.* Matter-wave interferometry in a double well on an atom chip. *Nature Phys.* **1**, 57–62 (2005).
4. Pethick, C. J. & Smith, H. *Bose–Einstein Condensation in Dilute Gases* (Cambridge Univ. Press, Cambridge, 2002).
5. Schöllkopf, W. & Toennies, J. P. Nondestructive mass selection of small van der Waals clusters. *Science* **266**, 1345–1348 (1994).
6. Arndt, M. *et al.* Wave-particle duality of C_{60} molecules. *Nature* **401**, 680–682 (1999).
7. Giulini, D. *et al. Decoherence and the Appearance of a Classical World in Quantum Theory* (Springer, Berlin, 1996).
8. Zurek, W. H. Decoherence, einselection, and the quantum origins of the classical. *Rev. Mod. Phys.* **75**, 715–775 (2003).
9. Hackermüller, L., Hornberger, K., Brezger, B., Zeilinger, A. & Arndt, M. Decoherence of matter waves by thermal emission of radiation. *Nature* **427**, 711–714 (2004).
10. Deachapunya, S. *et al.* Thermal and electrical properties of porphyrin derivatives and their relevance for molecule interferometry. *J. Chem. Phys.* **126**, 164304 (2007).
11. Wang, C.H.-T., Bingham, R. & Mendonca, J. T. Quantum gravitational decoherence of matter waves. *Class. Quant. Grav.* **23**, L59–L65 (2006).
12. Brezger, B., Arndt, M. & Zeilinger, A. Concepts for near-field interferometers with large molecules. *J. Opt. B* **5**, S82–S89 (2003).
13. Clauser, J. F. in *Experimental Metaphysics* (eds Cohen, R. S., Horne, M. & Stachel, J.) 1–11 (Kluwer Academic, New York, 1997).
14. Gronniger, G. *et al.* Electron diffraction from free-standing, metal-coated transmission gratings. *Appl. Phys. Lett.* **87**, 124104 (2005).
15. Keith, D. W., Ekstrom, C. R., Turchette, Q. A. & Pritchard, D. E. An interferometer for atoms. *Phys. Rev. Lett.* **66**, 2693–2696 (1991).
16. Carnal, O. & Mlynek, J. Young's double-slit experiment with atoms: A simple atom interferometer. *Phys. Rev. Lett.* **66**, 2689–2692 (1991).
17. Chapman, M. S. *et al.* Optics and interferometry with Na_2 molecules. *Phys. Rev. Lett.* **74**, 4783–4786 (1995).
18. Freimund, D. L., Aflatooni, K. & Batelaan, H. Observation of the Kapitza–Dirac effect. *Nature* **413**, 142–143 (2001).
19. Gould, P. L., Ruff, G. A. & Pritchard, D. E. Diffraction of atoms by light: The near-resonant Kapitza–Dirac effect. *Phys. Rev. Lett.* **56**, 827–830 (1986).
20. Nairz, O., Brezger, B., Arndt, M. & Zeilinger, A. Diffraction of complex molecules by structures made of light. *Phys. Rev. Lett.* **87**, 160401 (2001).
21. Cronin, A. D. & McMorran, B. Electron interferometry with nanogratings. *Phys. Rev. A* **74**, 061602(R) (2006).
22. Cahn, S. B. *et al.* Time-domain de Broglie wave interferometry. *Phys. Rev. Lett.* **79**, 784–787 (1997).
23. Brezger, B. *et al.* A matter-wave interferometer for large molecules. *Phys. Rev. Lett.* **88**, 100404 (2002).
24. Casimir, H. B. G. & Polder, D. The influence of retardation on the London–van der Waals forces. *Phys. Rev.* **73**, 360–372 (1948).
25. Brühl, R. *et al.* The van der Waals potential between metastable atoms and solid surfaces: Novel diffraction experiments vs. theory. *Europhys. Lett.* **59**, 357–363 (2002).
26. Fagan, P. J. *et al.* Production of perfluoroalkylated nanospheres from buckminsterfullerene. *Science* **262**, 404–407 (1993).
27. Gotsche, N., Ulbricht, H. & Arndt, M. UV–VIS absorption spectroscopy of large molecules for applications in matter wave interferometry. *Laser Phys.* **17**, 583–589 (2007).
28. Hornberger, K., Sipe, J. E. & Arndt, M. Theory of decoherence in a matter wave Talbot–Lau interferometer. *Phys. Rev. A* **70**, 053608 (2004).
29. Savas, T. A., Schattenburg, M. L., Carter, J. M. & Smith, H. I. Large-area achromatic interferometric lithography for 100 nm period gratings and grids. *J. Vac. Sci. Technol. B* **14**, 4167–4170 (1996).
30. Tamai, N. & Miyasaka, H. Ultrafast dynamics of photochromic systems. *Chem. Rev.* **100**, 1875–1890 (2000).

Acknowledgements

The project is supported by the Austrian FWF within the projects START Y177-2 and SFB F1505 and by the European Commission within the RTN network HPRN-CT-2002-00309. K.H. acknowledges support by the DFG Emmy-Noether program. M.M. and M.M. acknowledge support from the Swiss National Science Foundation (SNSF) and the Innovation Promotion Agency (CTI). We thank A. Zeilinger for lending us a continuous-wave laser.
Correspondence and requests for materials should be addressed to M.A.
Supplementary Information accompanies this paper on www.nature.com/naturephysics.

Author contributions

The interferometry work was carried out by S.G., L.H., A.S., H.U., M.G., F.G. and M.A. Analysis was carried out by K.H. and S.G. The nanogratings were prepared by T.S. in collaboration with L.H. S.G. and L.H. contributed equally to the experiment. M.M. and M.M. designed, synthesized and characterized the fluorinated azobenzene derivative with high vapour pressure.

Competing financial interests

The authors declare no competing financial interests.